

# Small-scale anisotropy and intermittency in high and low-latitude solar wind

A. Bigazzi<sup>1</sup>

*Departamento de Matemática Aplicada, Universidade do Porto, Portugal*

L. Biferale

*Dipartimento di Fisica and INFN, Università di Roma Tor Vergata, Italy.*

S.M.A.Gama

*CMUP and Departamento de Matemática Aplicada, Universidade do Porto, Portugal*

and

M. Velli<sup>2</sup>

*Jet Propulsion Laboratory, California Institute of Technology, CA USA*

## ABSTRACT

We analyze low and high-latitude fast solar wind data from the Ulysses spacecraft from 1992 to 1994 using a systematic method to analyse the anisotropic content of the magnetic field fluctuations. We investigate all available frequencies,  $1-10^{-6}$ Hz, for both high and low-latitudes datasets and are able to quantify the relative importance of the anisotropic versus the isotropic fluctuations. We analyse, up to sixth order, longitudinal, transverse and mixed magnetic field correlations. Our results show that strongly intermittent and anisotropic events are present in the solar wind plasma at high frequencies/small scales, indicating the absence of a complete recovery of isotropy. Anisotropic scaling properties are compatible for high and low-latitude data, suggesting a universal behaviour in spite of the different rate of evolution of the fast solar wind streams in the two environments.

*Subject headings:* interplanetary medium — methods: data analysis — methods: statistical — (Sun:) solar wind — turbulence

---

<sup>1</sup> Also visiting researcher, Dipartimento di Fisica, Università di Roma Tor Vergata, Italy.

<sup>2</sup> Also Dipartimento di Astronomia e Scienza dello Spazio, Università di Firenze, Italy

## 1. Introduction

The solar wind is an inhomogeneous, anisotropic and compressible magnetized plasma where both velocity and magnetic fields fluctuate over a broad range of frequencies and scales, see e.g. the reviews of Tu & Marsch (1995) and Horbury & Tsurutani (2001). Fluctuations may originate either from the nonlinear interactions between large-scale streams (Coleman 1966, 1968; Matthaeus et al. 1990) or by interacting Alfvén waves produced close to the Sun and carried by the wind, (Belcher & Davis 1971; Dobrowolny et al. 1980; Leamon et al. 1998). Observations of the radial evolution of magnetic fields in the inner heliosphere show the presence of fully developed turbulent spectra within a range of  $10^{-4} - 10^{-1}$  Hz (Bavassano et al. 1982).

The spectral index depends on the frequency range and on the distance from the Sun, varying from  $-1.2$  to  $-1.7$ . Low-frequency measurements are performed at around  $10^{-5} - 10^{-2}$  Hz (Coleman 1968), while high frequency measurements sample the range closer to  $10^{-2} - 10^{-1}$  Hz, (Bavassano et al. 1982; Leamon et al. 1998; Horbury & Balogh 2001). The spectral index tends to flatten closer to the Sun, indicating that turbulence is evolving in the solar wind. Phenomenological theory of hydrodynamic turbulence (Kolmogorov 1941) predicts a value of  $-5/3$  for the spectral index, while the theory of Alfvén wave-driven magnetohydrodynamic (MHD) turbulence of Iroshnikov (1963) and Kraichnan (1965), predicts a slope of  $-3/2$ . Neither prediction takes into account the possible influence of anisotropies and the presence of intermittency (Burlaga 1991, 1992; Marsch & Liu 1993; Carbone 1993; Feynman & Ruzmaikin 1994; Carbone, et al. 1995b; Horbury & Balogh 1997; Ruzmaikin et al. 1995; Bruno et al. 2003; Hnat et al. 2003; Bershadskii & Sreenivasan 2004), in a systematic way.

The presence of anisotropy makes it difficult to compare observed data with the two predictions, while the presence of intermittency tells us that the characteristics of the spectrum are not sufficient to characterize the system: higher order statistics need to be taken into account. In particular, spectral indices alone are insufficient to discriminate amongst turbulence models.

Anisotropy has been measured by various techniques involving the calculation of second order moments of the field either in the real or Fourier space, such as the variance matrix or the power spectra (Belcher & Davis 1971; Carbone et al. 1995). The eigenvector of the variance matrix corresponding to the minimum eigenvalue is usually known as the minimum variance direction. This direction is aligned with the large-scale mean field, indicating suppression of turbulence in that direction (Leamon et al. 1998; Bruno et al. 1999). Several MHD models incorporate at various levels the asymmetry of the spectral indices in the field-aligned (longitudinal) and transverse directions (Shebalin et al. 1983; Zank & Matthaeus

1992; Ng & Bhattacharjee 1996; Goldreich & Sridhar 1997; Matthaeus et al. 1998). Although this is a possible way to characterize anisotropy, second order longitudinal and transverse structure functions contain both anisotropic and isotropic contributions, as will be detailed later in Section 2. Those two contributions, always mixed, need proper treatment to be disentangled. A more systematic approach to analyse anisotropy is therefore important. Moreover, the relation between anisotropy and intermittency has not been investigated so far. Anisotropy and intermittency may also be important in the context of scattering of particles in the heliosphere (see e.g. Giacalone & Jokipii (1996))

We present in this paper a method for extracting in a systematic way, from the one-dimensional spacecraft data, information on the anisotropy and intermittency of the magnetic field fluctuations, and the interplay between them. We base our analysis on the behaviour of both diagonal and non-diagonal components of higher order structure functions. We have systematically compared isotropic and anisotropic fluctuations at different scales and for different magnetic correlation functions. We measure how fast isotropy is recovered at small scales, concerning both typical fluctuations of the order of the mean standard deviation, and highly intermittent events, affecting more the tails of the magnetic field probability density at all scales. We use Ulysses data of high speed streams at two different points along its orbit, at high and low latitudes, in order to assess the dependence on the large-scale properties of the small-scales anisotropic fluctuations, i.e. the issue of small-scales universality.

The paper is organized as follows. In Section 2 we present the set of observables needed to have a systematic control on the isotropic and anisotropic ensembles. In Section 3 we present our data set and in Section 4 the main results for both the low and high latitudes data. Section 5, summarizes our findings suggesting further possible investigations.

## 2. Anisotropy and Structure function analysis

Structure function decomposition into isotropic and anisotropic components has already been exploited with success in hydrodynamics, both for experimental and numerical data analysis (Arad et al. 1998, 1999; Kurien & Sreenivasan 2000; Biferale & Toschi 2001; Biferale & Vergassola 2001; Shen & Warhaft 2002b), see also Biferale & Procaccia (2004) for a recent review. In the latter case, the anisotropic contents of fully developed flow has been systematically analyzed. Anisotropic fluctuations of the velocity field have been shown to be characterized by anomalous scaling, thus explaining the higher than predicted anisotropy found in the gradient statistics, an effect known as “small-scales persistence of anisotropies” (Shen & Warhaft 2000, 2002; Biferale & Vergassola 2001). Some analytical results on the persistency of anisotropies for magnetic fields have also been obtained in the simplified case of passive

magnetic advection by stochastic velocity fields (Falkovich et al. 2001; Lanotte & Mazzino 1999; Arad et al. 2000). The ideal way to assess the relative isotropic/anisotropic contents at all scales is to perform a decomposition of the correlation functions, of order 2 and higher, over a suitable eigenbasis with definite properties under the group of three-dimensional spatial rotations (the SO(3) group), corresponding to spherical harmonics decomposition for the simpler case of scalars. In principle, one needs to distinguish among different anisotropic contributions corresponding to the different projections on the whole set of eigenfunctions (Arad et al. 1999). Spacecraft data are inherently one-dimensional, therefore not directly suitable to be fed into an SO(3) analysis, which requires the whole field in a 3D volume to be systematically worked out. However, we shall show how it is possible to construct correlation functions of different orders that have null projection over the isotropic ensemble, i.e. with a leading contribution coming only by its leading anisotropic content, if any (Kurien & Sreenivasan 2000; Staicu et al. 2003; Jacob et al. 2004).

Data analysis is based on a set of multi-scale correlation functions built upon different combinations of magnetic field components. The most general  $n$ th order correlation,  $S_{\alpha_1, \dots, \alpha_n}^{(n)}(\mathbf{r})$ , depending on single separation  $(\mathbf{r})$ , is built from the  $n$  spatial increments of magnetic field components:

$$S_{\alpha_1, \dots, \alpha_n}^{(n)}(\mathbf{r}) = \langle \delta_{\mathbf{r}} B_{\alpha_1} \delta_{\mathbf{r}} B_{\alpha_2} \cdots \delta_{\mathbf{r}} B_{\alpha_n} \rangle \quad (1)$$

where

$$\delta_{\mathbf{r}} B_{\alpha} \equiv B_{\alpha}(\mathbf{x} + \mathbf{r}) - B_{\alpha}(\mathbf{x}) \quad (2)$$

is the difference between the values of component  $B_{\alpha}$  at two different points a distance  $\mathbf{r}$  away. Brackets  $\langle \cdot \rangle$  in (1) indicate the average over the locations  $\mathbf{x}$ . Notice that in (1) we have assumed homogeneity but not isotropy, i.e. the correlation functions keep their explicit dependence on the full vector  $\mathbf{r}$ . The correlation function (1) includes both *isotropic* and *anisotropic* contributions:

$$S_{\alpha_1, \dots, \alpha_n}^{(n)}(\mathbf{r}) = S_{\alpha_1, \dots, \alpha_n}^{(n), iso}(\mathbf{r}) + S_{\alpha_1, \dots, \alpha_n}^{(n), aniso}(\mathbf{r}). \quad (3)$$

In principle, different anisotropic contributions exist and one would need to further distinguish among them. In this study we limit ourselves to disentangling the isotropic contributions from the anisotropic, without entering the more subtle problem of separating out all the different anisotropies (the interested reader may consult Biferale & Procaccia (2004) for a detailed illustration on how to proceed in this direction).

For  $n = 2$  and  $\alpha_1 = \alpha_2$  in (1), we get the well known positively defined second order structure function, connected to the energy spectrum  $E_{\alpha, \alpha}(\mathbf{k}) = \langle |\hat{B}_{\alpha}(\mathbf{k})|^2 \rangle$  via a Fourier transform. Another widely used form of (1) is the longitudinal structure function, obtained

by projecting all field increments along the separation versor,  $\hat{\mathbf{r}}$ :  $S_L^n(r) = \langle (\delta \mathbf{r} \cdot \hat{\mathbf{r}})^n \rangle$ . The general form of the tensor (1) for  $n = 2$  in the case of a fully isotropic and parity invariant statistics, is given by the combination of the separation vector  $\mathbf{r}$  and the only isotropic second order tensor, the unity matrix  $\delta_{\alpha,\beta}$ :

$$S_{\alpha_1, \alpha_2}^{(2),iso}(\mathbf{r}) = \langle \delta \mathbf{r} B_{\alpha_1} \delta \mathbf{r} B_{\alpha_2} \rangle^{iso} = a(r) \delta_{\alpha_1, \alpha_2} + b(r) r_{\alpha_1} r_{\alpha_2} \quad (4)$$

where  $a(r)$  and  $b(r)$  are two scalar functions depending only on the amplitude  $r = |\mathbf{r}|$ . Similarly, the expression for the fourth order isotropic tensors,  $S_{\alpha_1, \dots, \alpha_4}^{(4),iso}(\mathbf{r})$ , comprises three scalar functions,  $c(r), d(r), f(r)$ :

$$\begin{aligned} S_{\alpha_1, \alpha_2, \alpha_3, \alpha_4}^{(4),iso}(\mathbf{r}) &= \langle \delta \mathbf{r} B_{\alpha_1} \delta \mathbf{r} B_{\alpha_2} \delta \mathbf{r} B_{\alpha_3} \delta \mathbf{r} B_{\alpha_4} \rangle^{iso} = f(r) r_{\alpha_1} r_{\alpha_2} r_{\alpha_3} r_{\alpha_4} + \\ &+ c(r) (\delta_{\alpha_1, \alpha_2} \delta_{\alpha_3, \alpha_4} + \text{perm.}) + d(r) (\delta_{\alpha_1, \alpha_2} r_{\alpha_3} r_{\alpha_4} + \text{perm.}) \end{aligned} \quad (5)$$

Analogous expressions hold for higher order isotropic correlation functions. The key observation is that by a suitable choice of the combination of indices  $\alpha_1, \dots, \alpha_n$  and of the orientation  $\mathbf{r}$  one may have the isotropic components vanish at any order,  $n$  in (3). From now on, let us fix the separation distance in the direction  $\hat{\mathbf{x}}$  so that  $\mathbf{r} = (r_x, 0, 0)$ . For the case  $n = 2$ , when  $\alpha_1 \neq \alpha_2$ , the resulting isotropic components vanish. We therefore have three different second order correlation functions that are *purely anisotropic*. When the order  $n$  of the correlation function is *even* it is enough to take an *odd* number of field increments in two different directions to have a *purely anisotropic* observable. Therefore a possible set of purely anisotropic correlations have the form:

$$S_{\alpha, \beta}^{p, q}(r_x) = \langle \delta_{r_x} B_{\alpha}^p \delta_{r_x} B_{\beta}^q \rangle \quad (p + q = n) \quad (6)$$

with both  $p$  and  $q$  odd and such that  $p + q = n$ . The above  $n$ th order correlation has a vanishing isotropic component when the combinations of indices  $\alpha = x$  and  $\beta = y, z$  are taken.

Before presenting the results of our data analysis, let us briefly comment on the translation from time series to spatial signals in our dataset. Of course, as it is the case for all spacecraft data, we only have access to the time evolution of the magnetic field along the orbit. We therefore cannot make an explicit evaluation of simultaneous field increments over space. Nevertheless, the advecting velocity speed is so high (see next section for a summary of the main physical relevant quantities) that in the range of frequencies we are interested in, it is possible to safely adopt the Taylor hypothesis and translate time increments into spatial increments. The “Taylor hypothesis” consists in supposing the 3D field as frozenly advected by the underlying large scale velocity field,  $\mathbf{V}_0$  Frisch (1995). Field increments in the same spatial point at two times,  $t, t'$ , are considered equal to the instantaneous field increments

over two spatial locations  $\mathbf{x}$  and  $\mathbf{x} + \mathbf{r}$  with  $\mathbf{r} = \mathbf{V}_0(t' - t)$ . Therefore, for us, the direction  $\mathbf{r}$  is fixed and given by the direction of the wind at the location of the spacecraft that is, within a few percent, the spacecraft-Sun direction. This direction, as said before, will be taken as our reference  $\hat{\mathbf{x}}$  axis. Spatial homogeneity is translated via the Taylor hypothesis into temporal stationarity.

### 3. Ulysses Dataset

Ulysses orbit samples the interplanetary plasma at distances varying approximately from 1 to 6 A.U, on a polar orbit. It is therefore possible to follow the evolution of plasma characteristics with distance and latitude. We use two different set of data: the first one was taken by Ulysses during 1992-1993, when the spacecraft was at about 20° heliographic latitude and 5 AU distance from the Sun. The second was taken at the end of 1994, with Ulysses above the South Pole, at about 80° latitude and a distance of about 2 AU from the Sun. This latest dataset has just recently been made available to the community by the Ulysses team. Solar activity was, during the 92-93 period, declining, after the 1990 maximum. In 1994, the cycle was approaching the minimum of 1996. Each daily dataset provides the magnitude of all three components of the interplanetary magnetic field, taken at the rate of 1 or two seconds by the Vector Helium Magnetometer on board (Balogh et al., 1992). In Table 1 we report, for the two datasets, the interval of time considered, the heliographic latitudes spanned, distance from the Sun, average speed of the wind and average magnetic field intensity.

We pre-process data in order to clean spikes due to instrumental problems or to large shocks. This is made by excluding those data where the jump in the magnetic field between two consecutive data points (usually 1 second apart) is larger than a threshold,  $\Delta B$ , of the order of the mean large scale magnetic field. A fraction of datapoints as small as  $10^{-5}$ , is discarded this way. As a result, we can access magnetic field fluctuation on a range of

Table 1. Low latitudes and Polar datasets.

Dataset	Days	Lat (HGL)	Dist (A.U.)	Speed (Km s <sup>-1</sup> )	$\langle B \rangle$ (nT)
Low lat	92/209-93/137	-15 to -30	5.3 to 4.7	750	0.47
Polar	94/245-265	-79.7 to -80.2	2.37 to 2.23	760	1.3

frequencies of almost six decades.

In Table 2 we detail the total number of datapoints in the dataset, the number of datapoints discarded,  $N_{\text{excl}}$ , the fraction of the latter to the total, the threshold on the maximum jump between magnetic field for consecutive datapoints, the average field intensity for the whole dataset.

### 3.1. Low latitude dataset

The alternating pattern of slow and fast wind is shown in Fig. 1, spanning a ten month period, from day 209, 1992, to day 137, 1993. Within this period, we selected those sequences, of about five days each, when spacecraft is embedded in the trailing edges of high speed streams and velocity is above 650 Km/s. The days selected are, in 1992, 209-214, 235-241, 259-263, 337-342 and, in 1993, 28-34, 53-57, 81-85, 108-113, 133-137. They are highlighted in Fig. 1 within vertical lines.

### 3.2. High latitude dataset

Twenty-one consecutive days around the maximum latitude reached at perihelium, during the fast latitude scan of 1994, are selected. Differently from the previous dataset, only the fast component of the wind is present. Table 1 lists latitude range, distance, average speed and average magnetic field for this dataset as well.

Table 2. Data selection

Dataset	$N$	$N_{\text{excl}}$	$N_{\text{excl}}/N$	$\Delta B$ (nT)	$\langle B \rangle$ (nT)
Low latitude	3 915 792	78	2.0 E-5	0.5	0.47
High latitude	1 476 051	36	2.4 E-5	1.2	1.30

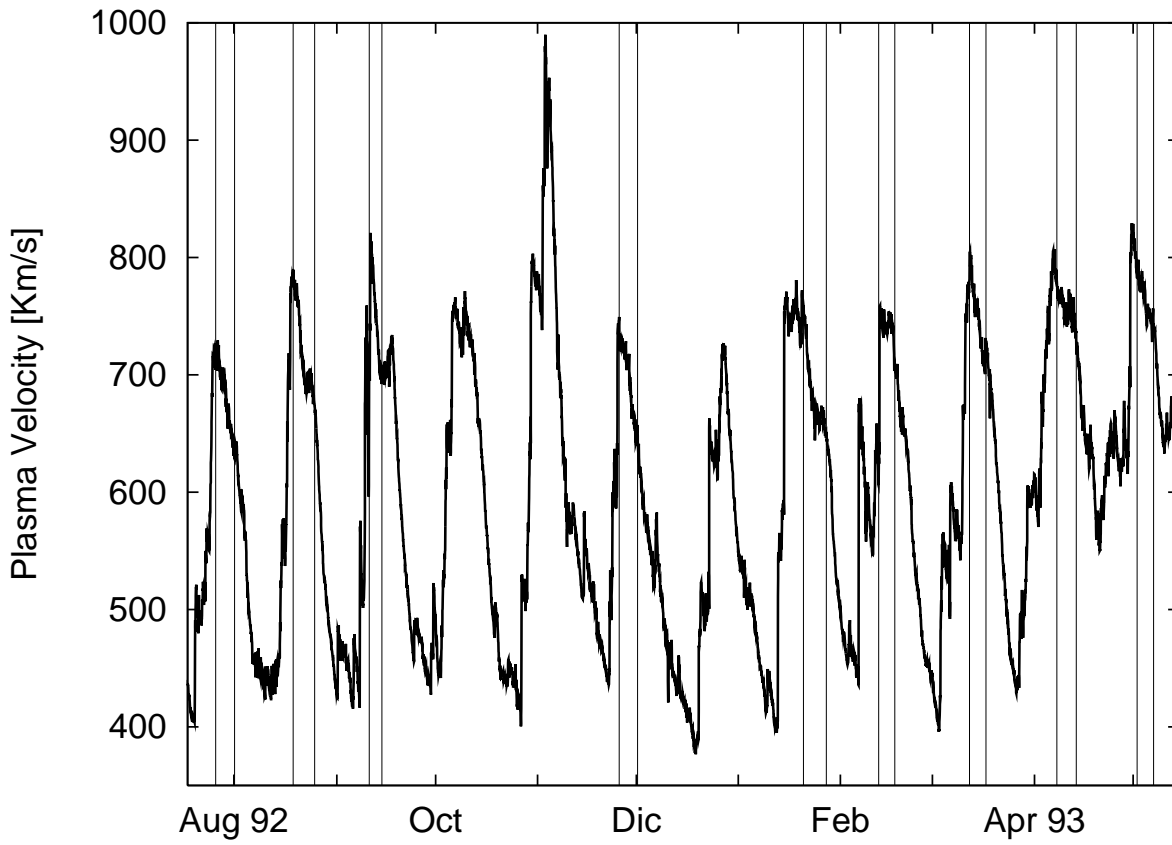


Fig. 1.— Plasma velocity sampled by Ulysses spacecraft between day 209 (July 27) 1992 and day 137 (May 17) 1993. Spacecraft was between  $-15^\circ$  to  $-30^\circ$  heliographic latitude, approaching the Sun at a distance varying from 5.3 to 4.7 AU (see Table 1). Vertical lines highlight selected intervals in the trailing edges of high-speed streams.

## 4. Results

### 4.1. Equatorial data

We want to first test the consistency between the disjoint sets making up the low latitude dataset of Fig. 1. The second order longitudinal structure functions, calculated for each of those intervals of contiguous data, are shown in Fig. 2. They are consistent with each other over more than 5 decades, from 1 to  $10^5$  Hz in the spacecraft frame, which translates, with a mean plasma velocity of 750 Km/s, into a range of  $7.5 \cdot 10^{-1}$  Mm to  $7.5 \cdot 10^4$  Mm. Some intervals have a more intense signal than others do.

The anisotropic component  $S_{xz}^{(2)}$  shown in the inset of the same figure, displays a similar behavior. We conclude that data from different intervals are commensurable and combine them together to obtain more stable statistical results. We shall refer to the combined set as the “low-latitude” dataset without further distinction.

Let us now compare the undecomposed second order structure functions with its anisotropic content. In Fig.3 we plot the longitudinal structure functions of second order,  $S_{x,x}^{(2)}(r_x)$  and the two transverse structure functions in the directions perpendicular to the  $\hat{x}$  axis,  $S_{yy}^{(2)}(r_x)$  and  $S_{zz}^{(2)}(r_x)$ . All these functions have both isotropic and anisotropic contribution:

$$S_{\alpha,\alpha}^{(2)}(r_x) = S_{\alpha,\alpha}^{(2),iso}(r_x) + S_{\alpha,\alpha}^{(2),aniso}(r_x) \quad (7)$$

The two *purely anisotropic* second order structure functions  $S_{xy}^{(2)}(r_x)$  and  $S_{xz}^{(2)}(r_x)$ , are plotted in the same figure. A few comments are in order. First, we notice that the *anisotropic* correlations have a smaller amplitude with respect to the full correlation functions. This suggests that the isotropic contribution in the decomposition (3) is dominant. Moreover, we see that the anisotropic curves decay slightly faster than the full correlation by decreasing the scale. In other words, isotropic fluctuations become more leading going to small scales, but very slowly. This is consistent with the *recovery-of-isotropy* assumption often advocated in many phenomenological theory of hydrodynamic turbulence and magnetized plasma. However, in order to assess more precisely this issue, it is important to control higher order statistical objects, i.e. the whole shape of the probability density distribution, at all scales. In the inset of the same Fig. 3 we show the same comparison between longitudinal,  $S_{xxxx}^{(4)}(r_x)$ , transverse,  $S_{\alpha\alpha\alpha\alpha}^{(4)}(r_x)$  (with  $\alpha = y, z$ ) and *purely anisotropic* correlations of *fourth order* (see caption in the figure). Now the situation is quite different. First, the intensity of some *purely anisotropic* components are much closer to those with mixed isotropic and anisotropic contributions, i.e. the longitudinal and transverse structure functions. Second, the decay rate as a function of the scale is almost the same: no recovery of isotropy is any more detected for fluctuations of this order. A similar, even more pronounced, trend is observed for sixth order quantities (not

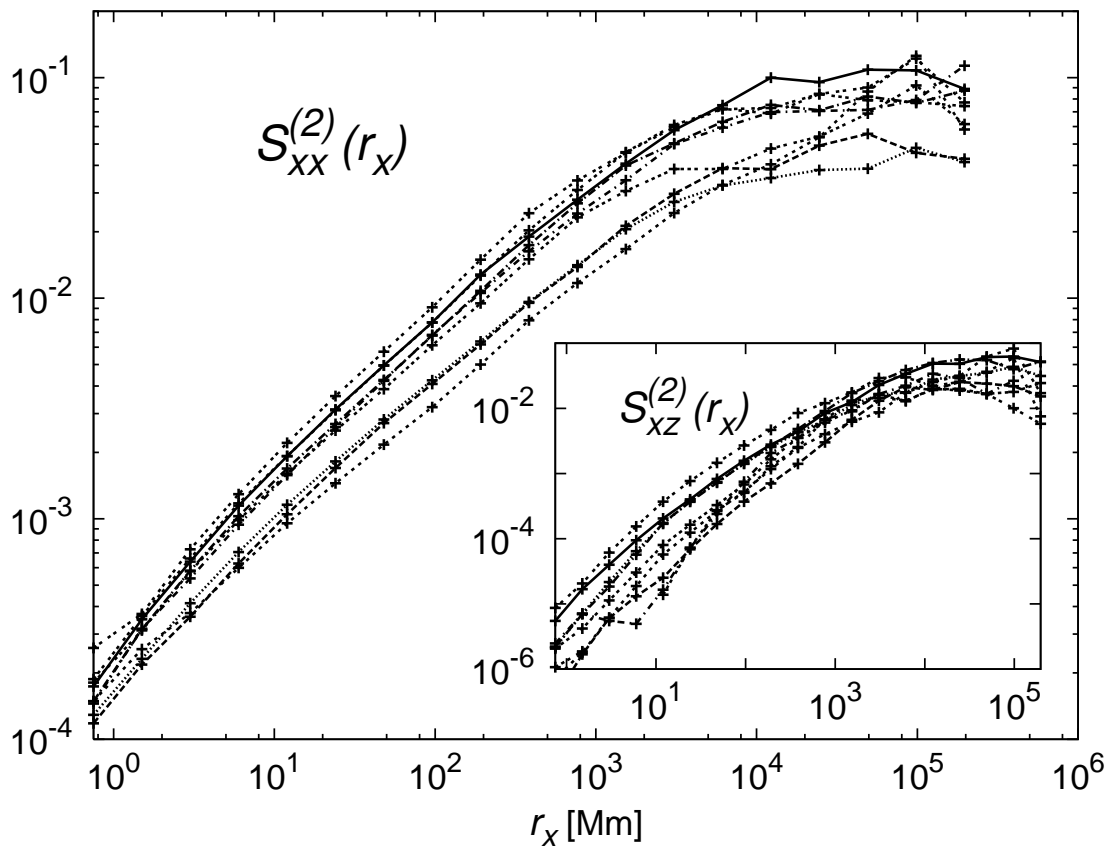


Fig. 2.— Second order longitudinal structure function,  $S_{xx}^{(2)}(r_x)$ , for each interval comprising the low latitude dataset (see Fig. 1), as a function of the separation  $r_x$ . In the inset, the second order purely anisotropic structure function,  $S_{xz}^{(2)}(r_x)$ .

shown). The persistence of strong anisotropies at high frequencies (small scales) cast some caveat on measurements of quantities which do not properly disentangle the isotropic from the anisotropic components. As it will be shown later for the case of high-latitudes data, anisotropic components have strong variations in intensity depending on the position on the solar orbit. Both latitude and distance from the Sun influence the amount of anisotropy. As a result, undecomposed quantities which are influenced by both isotropic and anisotropic fluctuations are expected to be non-universal, the anisotropic content being dependent on the spacecraft position and latitude. This must hold for the spectrum and even more for higher order structure functions.

## 4.2. Intermittency

Anisotropic fluctuations are not the unique source of complexity in solar wind data. It is well known that both magnetic and velocity fields are strongly intermittent, i.e. their statistical properties at different scales cannot be simply superimposed by rescaling. This implies the existence of anomalous scaling laws in the structure functions and “fat tails” in the PDFs of field increments Frisch (1995). Here we want to address this issue for the anisotropic sectors. The main conclusion will be that anisotropic correlations also show anomalous scaling, their PDFs becoming more and more non-Gaussian at small scales. In Fig. 4 we show the Kurtosis of both the longitudinal and transverse structure functions, i.e. the ratio between fourth order moments and square of the second order moments of longitudinal and transverse increments:

$$K_{\alpha}^{(4)}(r_x) = \frac{S_{\alpha\alpha\alpha\alpha}^{(4)}(r_x)}{(S_{\alpha\alpha}^{(2)}(r_x))^2} \quad (8)$$

A Gaussian variable would have a Kurtosis of 3, independent on the scale while all three curves grow at small scales. We stress once more here that these quantities probe both the iso and anisotropic physics. Therefore the scaling properties are certainly affected by the superposition of different contributions. In the previous section we have shown that the isotropic sector is never sub-leading. We may therefore consider the above result as a confirmation that the isotropic fluctuations are indeed strongly intermittent.

Similarly, to investigate intermittency in the anisotropic sector, it is useful to define a *purely anisotropic* Kurtosis, by taking the adimensional ratios of fourth order and second order anisotropic correlation functions:

$$K_{\alpha\beta}^{(4),aniso}(r_x) = \frac{S_{\alpha\beta\beta\beta}^{(4)}(r_x)}{(S_{\alpha\beta}^{(2)}(r_x))^2} \sim r_x^{\chi_4^{aniso}} \quad (9)$$

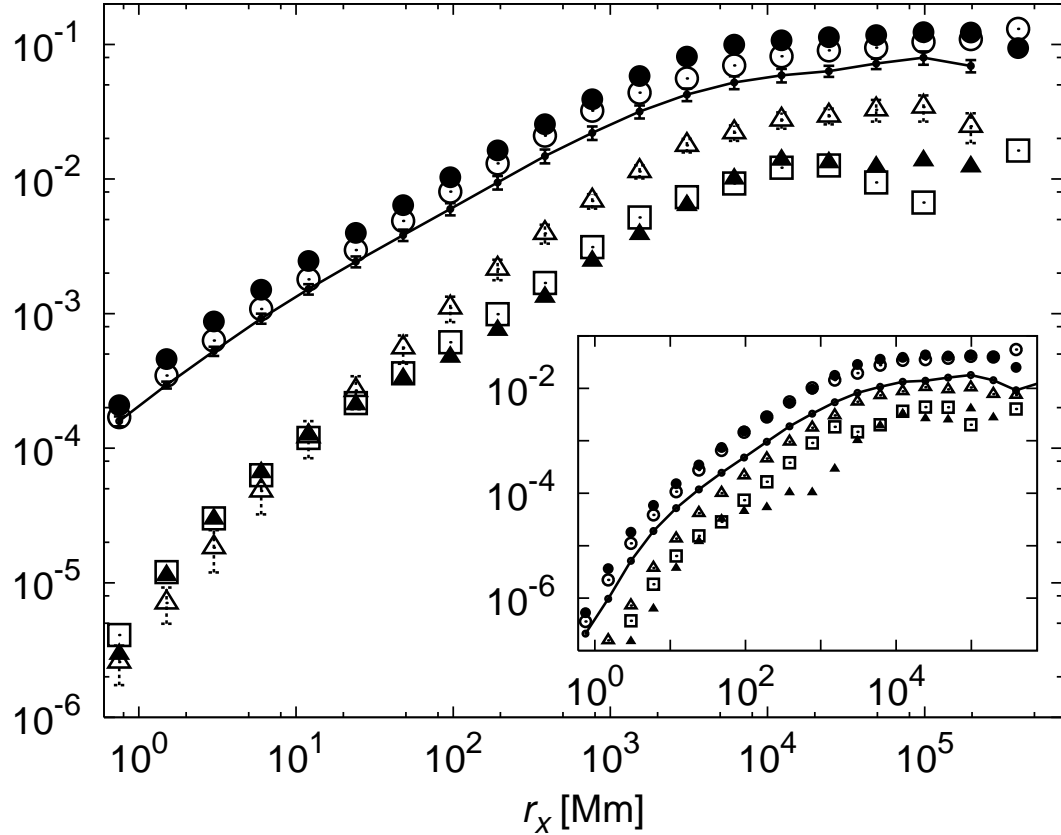


Fig. 3.— Second order longitudinal, transverse and *purely anisotropic* structure functions. Low latitude dataset. The upper three curves show the longitudinal and transverse structure functions: solid line —  $S_{xx}^{(2)}$ ; empty circles  $\circ$   $S_{yy}^{(2)}$ ; filled circles  $\bullet$   $S_{zz}^{(2)}$ . Errorbars are superimposed on —  $S_{xx}^{(2)}$ . Errors are evaluated as the standard deviation of the individual intervals comprising the whole dataset. The lower curves show the purely anisotropic structure functions:  $S_{xy}^{(2)}$ ,  $\blacktriangle$  filled triangles;  $S_{xz}^{(2)}$ ,  $\triangle$  empty triangles;  $S_{yz}^{(2)}$ ,  $\square$  empty squares. Errorbars are superimposed on  $\triangle S_{xz}^{(2)}$ . Inset: fourth order structure functions, longitudinal, transverse and *purely anisotropic*. Solid line, —  $S_{xxxx}^{(4)}$ ; empty circles  $\circ$   $S_{yyyy}^{(4)}$ ; filled circles  $\bullet$   $S_{zzzz}^{(4)}$ . *Purely anisotropic* structure functions are:  $S_{xyyy}^{(4)}$ ,  $\blacktriangle$  filled triangles;  $S_{xzzz}^{(4)}$ ,  $\triangle$  empty triangles;  $S_{yzzz}^{(4)}$ ,  $\square$  empty squares.

where  $\alpha, \beta$  are chosen so that contributions from the isotropic sector in both the numerator and the denominator vanish. The anisotropic components of the kurtosis (9) are shown in the inset of Fig. 4. Functions are increasing towards small scales, with slopes of  $\chi_4^{(aniso)} = -0.6 \pm 0.2$ ,  $\chi_4^{(aniso)} = -0.8 \pm 0.2$ ,  $\chi_4^{(aniso)} = -0.45 \pm 0.2$  for the  $xy$ ,  $xz$  and  $yz$  components, respectively (see Table 3). This is the first clear indication, to our knowledge, that anisotropic fluctuations in the solar plasma are strongly intermittent. Similar trends are observed for generalized Kurtosis of sixth order (not shown):

$$K_{\alpha\beta}^{(6),aniso}(r_x) = \frac{S_{\alpha\alpha\alpha\beta\beta\beta}^{(6)}(r_x)}{(S_{\alpha\beta}^{(2)}(r_x))^3} \sim r_x^{\chi_6^{(aniso)}} \quad (10)$$

There, our best estimate for the exponents is  $\chi_6^{(aniso)} = -1.2 \pm 0.3$ ,  $xy$  component, and  $\chi_6^{(aniso)} = -1.5 \pm 0.3$ ,  $xz$  component.

Let us here remark that the quantity in (9) is not constructed from ratios of 4th and 2nd order moments of the same observable, i.e. it is not, rigorously speaking, the kurtosis of a stochastic variable. Nevertheless, it is a good probe of the relative intensity of 4th versus 2nd order anisotropic moments, the best that can be done with a one-dimensional set of data.

A power law fit of the numerator and denominator of (9,10) can be used to directly measure the scaling exponents of the second order,

$$S_{\alpha\beta}^{(2)}(r_x) \sim r_x^{\zeta_2^{(aniso)}}, \quad (11)$$

and higher order anisotropic correlation functions,

$$S_{\alpha\beta\beta\beta}^{(4)}(r_x) \sim r_x^{\zeta_4^{(aniso)}} \quad S_{\alpha\alpha\alpha\beta\beta\beta}^{(6)}(r_x) \sim r_x^{\zeta_6^{(aniso)}} \quad (12)$$

with, as customary now,  $\alpha, \beta$  are chosen in such a way that only *purely anisotropic* quantities are returned. We found  $\zeta_2^{(aniso)} = 0.75 \pm 0.1$  for the  $xy$  component,  $\zeta_2^{(aniso)} = 0.95 \pm 0.1$  for the  $xz$  component, and  $\zeta_2^{(aniso)} = 0.75 \pm 0.1$  for the  $yz$  component, see Table 3. Values for the fourth and sixth orders  $\zeta_4^{(aniso)}$  and  $\zeta_6^{(aniso)}$  may also be read out from the same table. Errorbars are estimated from the change of slope in the range of scales from 10 to  $10^3$  Mm. Missing entries in the table indicate that the scaling properties were not well defined within that range.

The above results show that anisotropic fluctuations, although they never become the leading ones are still important at small scales. Order by order, the undecomposed correlation function is more intense than any anisotropic projection. This can be visualized, for the 4th

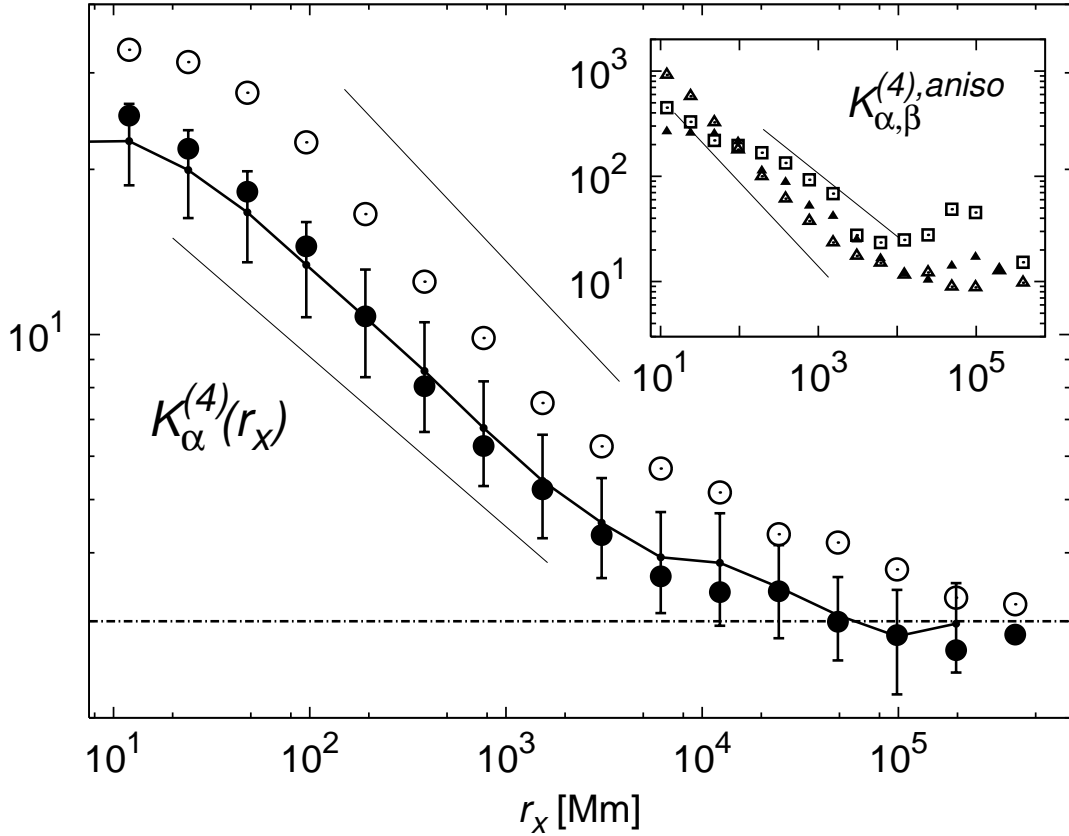


Fig. 4.— Kurtosis (8) of longitudinal and transverse magnetic field fluctuations. Solid line —  $K_x^{(4)}(r_x)$ ; empty circles  $\circ K_y^{(4)}(r_x)$ ; filled circles  $\bullet K_z^{(4)}(r_x)$ . Straight lines represent linear fit to the central portion of the curves with slopes of  $-0.31$  for the longitudinal component, and  $-0.38$  for the two transverse ones. The horizontal line corresponds to the Gaussian value of  $3$ , attained only at large scales. In the inset: *purely anisotropic* kurtosis (9).  $K_{xy}^{(4)}(r_x)$ ,  $\blacktriangle$  filled triangles;  $K_{xz}^{(4)}(r_x)$ ,  $\triangle$  empty triangles;  $K_{yz}^{(4)}(r_x)$ ,  $\square$  empty squares. Straight lines have slopes of  $\chi_4^{aniso} = -0.8$  and  $\chi_4^{aniso} = -0.6$  in the  $xz$  and  $xy$  components, respectively. Low latitude dataset.

and 6th orders, by plotting the ratio between the undecomposed object and one anisotropic projection:

$$G_{xz}^{(4)}(r_x) = \frac{S_{xzzz}^{(4)}(r_x)}{S_{xxxx}^{(4)}(r_x)}; \quad G_{xz}^{(6)}(r_x) = \frac{S_{xxxxzzz}^{(6)}(r_x)}{S_{xxxxxx}^{(6)}(r_x)} \quad (13)$$

These quantities never increase at small scales, indicating that isotropic contribution in the denominator is leading with respect to the anisotropic, see Fig. 5. Another quantity that can be used to characterize the relative weight of anisotropic to isotropic fluctuations, may be built from a  $n$ th order anisotropic moment and the  $n/2$  power of a 2nd order isotropic moment (Shen & Warhaft 2002b; Biferale & Vergassola 2001). For example, in our geometry, one possible choice would be:

$$F_{xz}^{(4)}(r_x) = \frac{S_{xzzz}^{(4)}(r_x)}{(S_{xx}^{(2)}(r_x))^2} \quad F_{xz}^{(6)}(r_x) = \frac{S_{xxxxzzz}^{(6)}(r_x)}{(S_{xx}^{(2)}(r_x))^3} \quad (14)$$

where the numerator is a *purely anisotropic*  $n$ th order quantity while the denominator is the 2d order longitudinal structure function, raised to the  $n/2$  power. Clearly all quantities in (13) and (14) would be vanishing in a perfect isotropic ensemble. The difference between the two definitions (13) and (14) for  $F$  and  $G$ , lies in the normalizing function in the denominator. In the first case,  $G$ , the normalization is through a correlation of the same order of the numerator while in the second case,  $F$ , is via a second order correlation raised to the appropriate power. Their amplitude as a function of  $r_x$  can be taken as a measure of the change in the anisotropic content as a function of scale. The defintion (14), on the other hand, mixes correlation of different orders, thus including their possible different intermittent corrections (Biferale & Vergassola 2001). In Fig. 5 we also show the behavior of  $F_{xz}^{(n)}(r_x)$  for  $n = 4, 6$ . Again, there is a clear indication of the presence of important anisotropic contributions, particularly at small scales.

### 4.3. Probability density functions

Before concluding this section we want to re-discuss some of the previous results from the point of view of the probability density functions (PDFs). Anisotropies may be highlighted at the level of the PDF by looking at the antisymmetric part of the distribution of field increments at different scales. Let us define the PDF,  $P(X_{\alpha\beta})$ , of the dimensionless magnetic field increments at scale  $r_x$ :

$$X_{\alpha\beta}(r_x) = \frac{\delta_{r_x} B_\alpha \delta_{r_x} B_\beta}{\langle \delta_{r_x} B_x \delta_{r_x} B_x \rangle}. \quad (15)$$

In order to make the stochastic variable dimensionless we have normalized it with the longitudinal second order structure functions at that scale. With a suitable choice of the indices

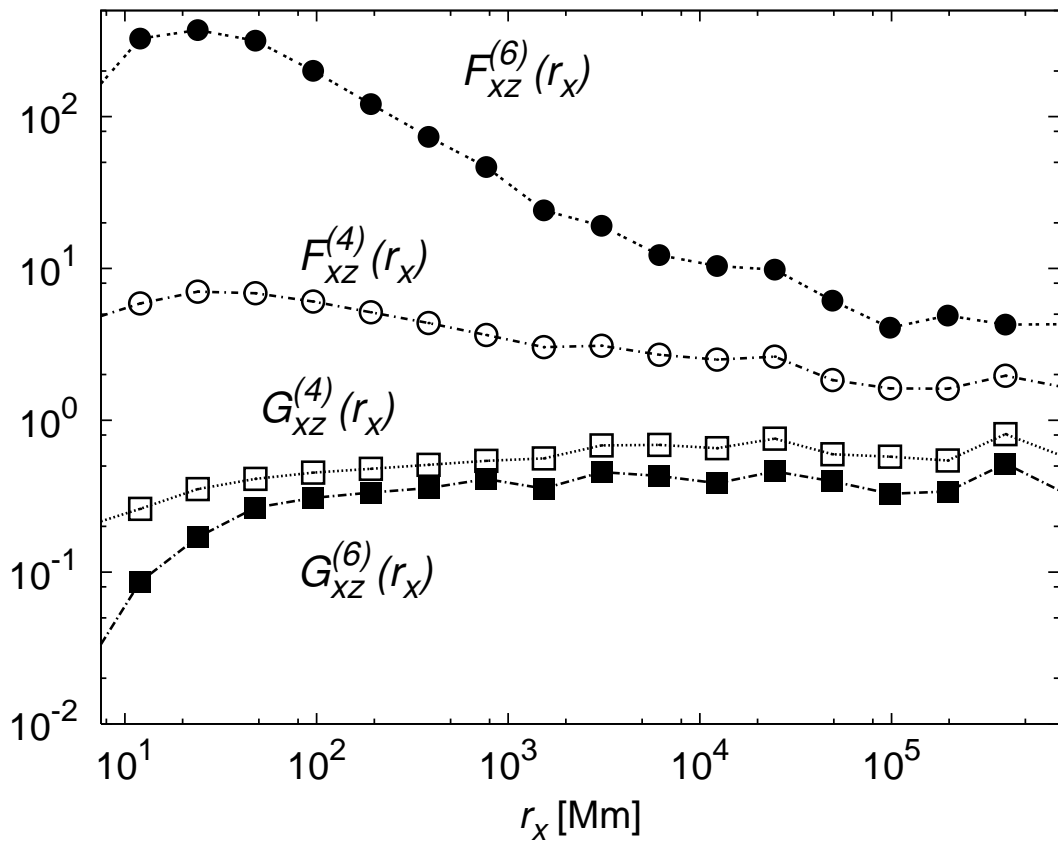


Fig. 5.— Generalized flatness  $G_{\alpha\beta}^{(n)}(r_x)$  and  $F_{\alpha\beta}^{(n)}(r_x)$  of order 4 and 6, Eqs. (13) and (14) for components  $xz$  and  $xy$ . Low latitude dataset.

$\alpha\beta$ , all odd moments of  $X_{\alpha\beta}(r_x)$  would be zero in a perfectly isotropic ensemble. This is the case when  $\alpha = x$  and  $\beta = y, z$ . We may now define the antisymmetric part of  $P(X_{\alpha\beta})$  as

$$A_r(X_{\alpha\beta}) = P(X_{\alpha\beta}(r_x)) - P(-X_{\alpha\beta}(r_x)), \quad (16)$$

and notice that it would vanish in a symmetric isotropic ensemble.

$A_r(X_{\alpha\beta})$  gives us a direct measurement of the anisotropy as the imbalance in the probability of having oppositely directed fluctuations at that scale. In Fig. 6 we show the anti-symmetric part of the PDF,  $A_r(X_{\alpha\beta}(r_x))$  for  $\alpha = x$  and  $\beta = z$  for three different separations  $r_x$ . The increasingly fat tails as one goes to smaller scales, reflects the non-gaussianity of  $P(X_{xz}(r_x))$ , which becomes more enhanced at small scales. In order to assess the relative weight of the antisymmetric versus the symmetric fluctuations, we define the normalised antisymmetric part of  $P(X_{\alpha\beta})$ :

$$R_x(X_{\alpha\beta}) = \frac{P(X_{\alpha\beta}(r_x)) - P(-X_{\alpha\beta}(r_x))}{P(X_{\alpha\beta}) + P(-X_{\alpha\beta})}, \quad (17)$$

This quantity also vanish in a symmetric isotropic ensemble, approaching the value one in the limit case of strong anisotropy,  $P(X_{\alpha\beta}) \gg P(-X_{\alpha\beta})$ . In the inset of the same figure,  $R(X_{xz})$  is shown. The fact that at large separations  $R(X_{xz})$  is close to one, means that large events are progressively more anisotropic as they grow in intensity, a possible signature of the large scale structures in the plasma. For small separations, the system is indeed globally more isotropic, although small scale anisotropy never vanish and survives at a significant level of 10% for all intensities.

#### 4.4. High-latitudes data

We discuss here anisotropy and intermittency detected in the polar region by Ulysses. This allows us to address the “universality” of anisotropy, i.e. quantifying to which extent intensities of anisotropic fluctuations and their scaling properties are dependent/independent on the mean large scale structure on the magnetized plasma. There are two effects which might influence the relative anisotropy of the turbulence in the polar and equatorial regions. In the polar regions, the amplitude of turbulence relative to the mean field is stronger, while the effects of solar rotation, which tend to bend the interplanetary magnetic field into a spiral, are negligible. In the equatorial high speed streams, the average magnetic field is bent into the Parker (spiral) direction, so that there are two main axes which may influence the evolution of the fluctuations, the radial and the mean field directions. The mean field direction coincides with the radial direction for polar flows while it is perpendicular to it, close to the  $y$  direction, for the low-latitude data around 5 A.U.

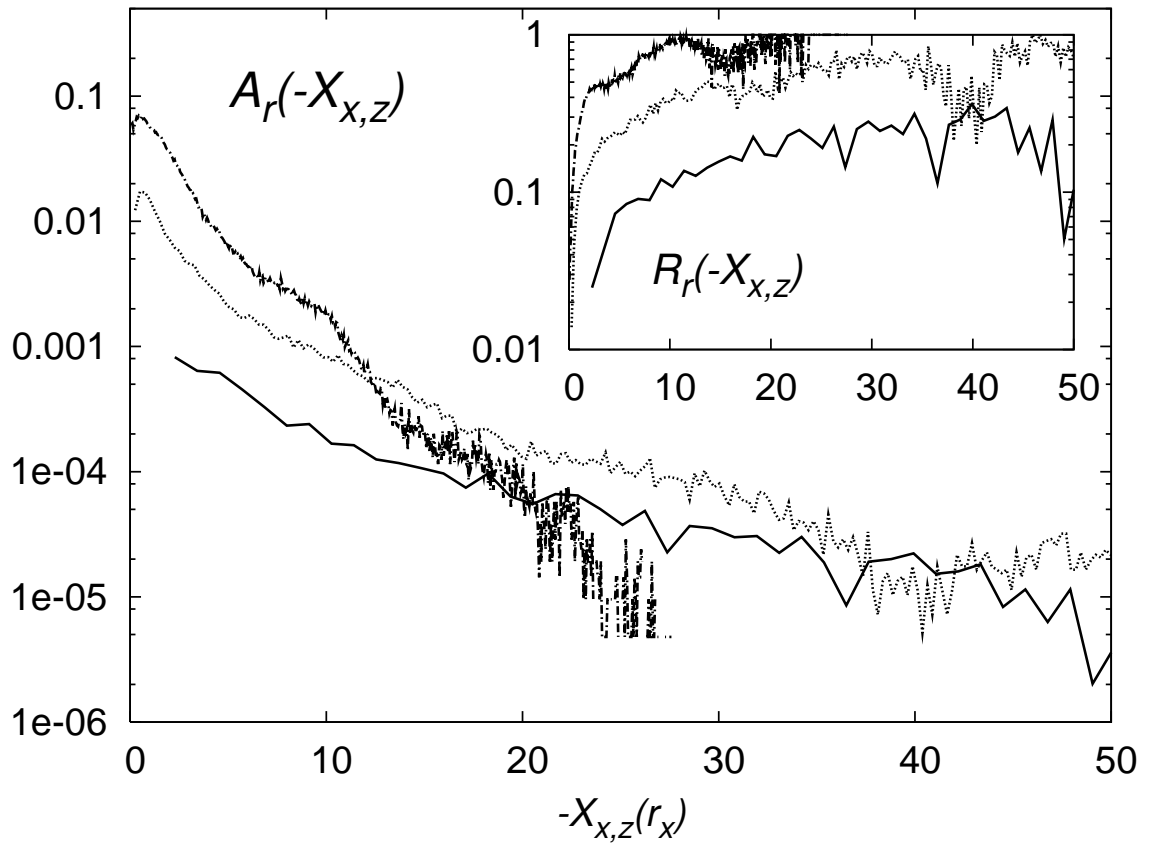


Fig. 6.— Antisymmetric part of the PDF of  $X_{xz}(r_x)$ ,  $A_r(-X_{xz})$  Eq. (16), for three different spatial separations  $r$ . Solid line:  $r = 12$  Mm, dotted line:  $r = 192$  Mm, dot-dashed line:  $r = 3072$  Mm. Inset: the normalised antisymmetric part of the PDF,  $R_r(-X_{xz})$ , Eq. (17), for the same set of  $r_x$ .

Let us first present results on the overall relative importance of anisotropic fluctuation with respect to the undecomposed ones. In Fig. (7) we show the same as in Fig. (3) but for polar data. *Purely anisotropic* structure functions have a much lower intensity (one order of magnitude less) with respect to the longitudinal and transverse structure functions both for the second order (body of the figure) and for the fourth order (inset). Indeed, for higher order moments, 6 and higher, the statistical fluctuations combined with the very low intensity of the anisotropic signal do not allow to have stable results even with the whole statistic of 21 consecutive days we analyzed. We conclude therefore that the anisotropy content at this latitude is much lower than in the low latitude dataset. One could argue that at this latitudes averaging over long periods may hide important physical phenomena which appear on a shorter time window. Therefore, we also selected periods of 2-3 consecutive days when the anisotropic signal looked more stable and intense. The anisotropic content in those events is slightly more important and allow to make a quantitative estimate of its scaling properties, but do not differ qualitatively. In Table 3, data with an asterisk \* indicate that scaling exponents are evaluated on the smaller dataset.

In Fig. (8) we show the same as Fig. (4), for the polar data set. We show the Kurtosis of longitudinal and transverse magnetic field fluctuations together with the Kurtosis for *purely anisotropic* correlation functions (9). Comparing the scaling behaviours of all the statistical indicators considered, summarized in Table 3, we have a qualitative agreement between the polar and the “Equatorial” data set. If confirmed by other measurements, and/or with higher statistical data sets, this would be a nice indication of “universality” in the small scales fluctuations of the solar wind plasma. Overall intensities of isotropic and anisotropic contents are of course dependent on the distance and latitude, while their variation with scale/frequency look more stable.

## 5. Conclusions

Our main finding is the detection of strong anisotropic fluctuations in the equatorial part of the orbit. Here, the anisotropic contents of fourth order correlation function is roughly of the same order of its isotropic part, at all scales, indicating that small scale isotropy is not recovered. Moreover, a high degree of intermittency is measured in the purely anisotropic fluctuations. In the polar region, anisotropies are smaller and highly fluctuating in time, but with a spatial dependencies compatible, within statistical errors, with the one observed at low latitudes. This would indicate some universal features of anisotropic solar fluctuations independently of the latitude, at least for what concerns their scaling properties. Our results point toward a crucial role played by anisotropic fluctuations in the small scales statistics.

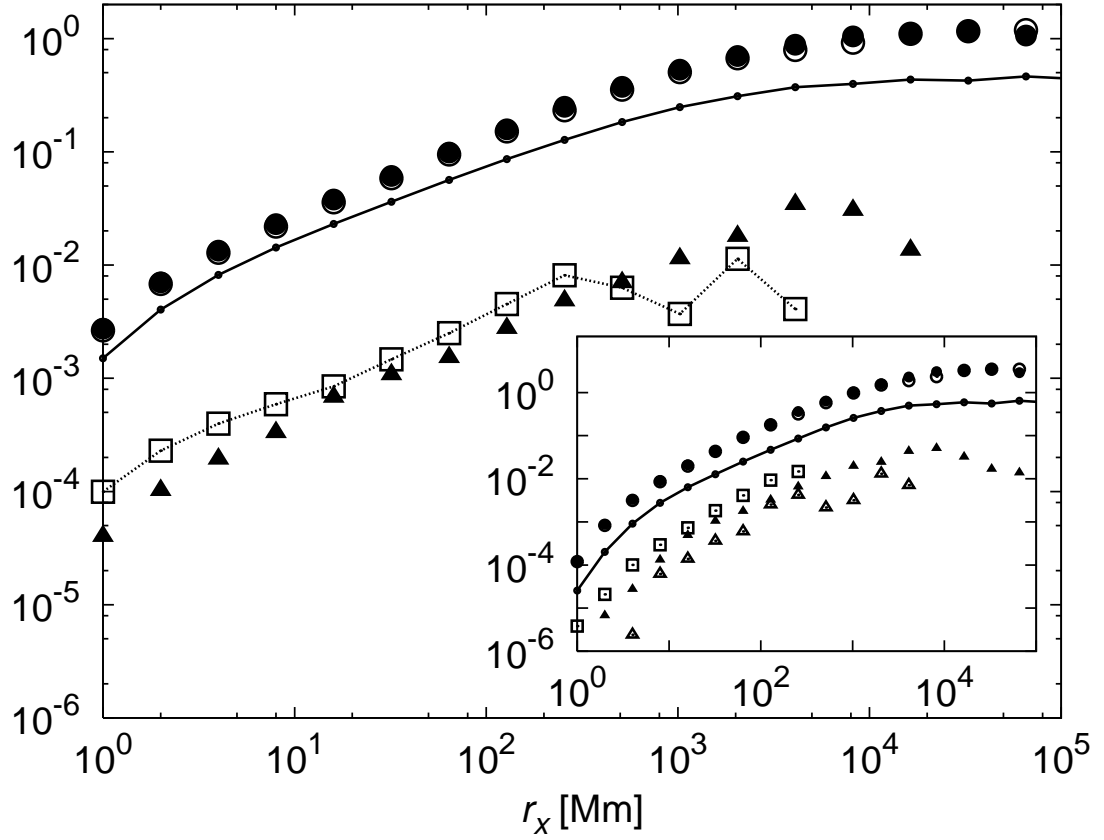


Fig. 7.— Same as in Fig. (3). Polar dataset. Second order longitudinal, transverse and *purely anisotropic* structure functions. The upper three curves show the longitudinal and transverse structure functions: solid line —  $S_{xx}^{(2)}$ , empty circles  $\circ$   $S_{yy}^{(2)}$  and filled circles  $\bullet$   $S_{zz}^{(2)}$ . The lower curve with triangles show the largest purely anisotropic structure functions:  $S_{xy}^{(2)}$ ,  $\blacktriangle$  filled triangles;  $S_{yz}^{(2)}$ ,  $\square$  empty squares. Inset: fourth order structure functions, longitudinal, transverse and *purely anisotropic*. Solid line, —  $S_{xxxx}^{(4)}$ , empty circles  $\circ$   $S_{yyyy}^{(4)}$ , filled circles  $\bullet$   $S_{zzzz}^{(4)}$ . *Purely anisotropic* structure functions are:  $S_{xyyy}^{(4)}$ ,  $\blacktriangle$  filled triangles;  $S_{xzzz}^{(4)}$ ,  $\triangle$  empty triangles;  $S_{yzzz}^{(4)}$ ,  $\square$  empty squares.

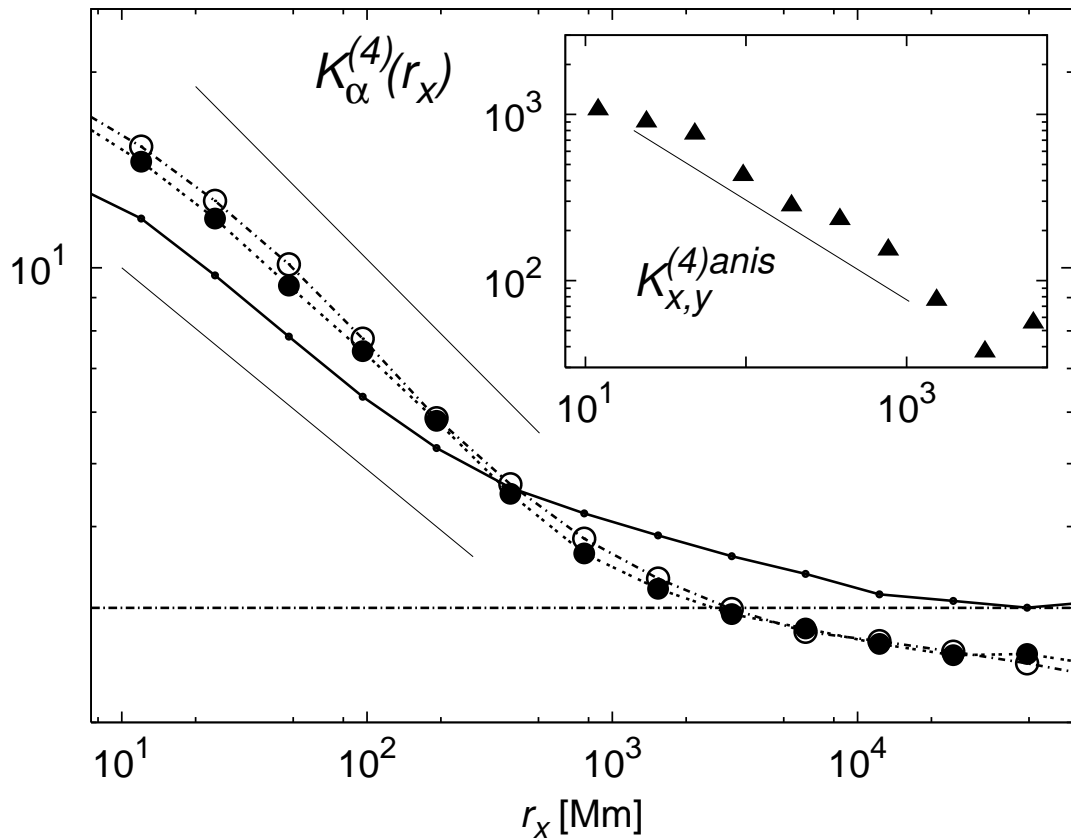


Fig. 8.— Same as in Fig. (4). Polar dataset. Kurtosis (8) of the longitudinal and transverse magnetic field fluctuations. Solid line —  $K_x^{(4)}(r_x)$ , empty circles  $\circ$   $K_y^{(4)}(r_x)$  and filled circles  $\bullet$   $K_z^{(4)}(r_x)$ . The dot-dashed line shows the constant level of three for the kurtosis of a Gaussian variable. In the inset: *purely anisotropic* kurtosis (9) of component  $\blacktriangle$   $K_{xy}^{(4)}(r_x)$ .

Models where higher order statistic is also taken into account, providing estimates for the scaling exponents of higher order anisotropic structure functions, will be important to a deeper understanding of solar wind turbulence.

Before concluding, let us go back to the issue of distinguishing different anisotropic fluctuations. As one learns from the theory of group of rotation in three dimensions, there is not a unique “anisotropic” sector, rather different anisotropic properties are described by projection on the eigenfunctions with different total angular momentum,  $j$ , and projections of the total angular momentum on a given axis,  $m$ , Arad et al. (1999). As mentioned in the introduction, the exact decomposition in different anisotropic sectors is possible only if using numerical data, providing access to the whole magnetic field in the 3D space. Here we have described the procedure that should be adopted for one-dimensional strings of data, extracting the “whole” anisotropic components out of the experimental data. This implies that all the estimate of scaling properties as here reported may well be affected by out-of-control contributions from different anisotropic sectors. The hope is that out of all anisotropic sectors, only the leading one is dominating the statistics at small scales. This hypothesis, which implies a hierarchy between the scaling exponents in different sector has been verified on direct numerical simulations of turbulent flows Biferale & Toschi (2001); Biferale et al. (2002) and on analytical calculation for passive magnetic fields Lanotte & Mazzino (1999); Arad et al. (2000), but remains an open question for active magnetic fields.

We are thankful to B. Bavassano, R. Bruno, A. Lanotte and F. Toschi for fruitful discussions. We acknowledge support from EU under the grant “Nonideal Turbulence” HPRN-CT-2000-0162.

## REFERENCES

Arad, I., Dhruva, B., Kurien, S., L'vov, S.V., Procaccia, I., & Sreenivasan, K. R., 1998, Phys. Rev. Lett., 5330.

Arad, I., L'vov, V. & Procaccia, I., 1999, Phys. Rev. E 59, 6753

Arad, I., Biferale, L. & Procaccia, I., 2000, Phys. Rev. E 61, 2654

Balogh, A., Beek, T. J., Forsyth, R. J., Hedgecock, P. C., Marquedant, R. J., Smith, E. J., Southwood, D. J., & Tsurutani, B. T. 1992, Astronomy and Astrophysics Supplement Series, 92, 221

Barnes, A., 1979, in Solar System Plasma Physics, Vol. 1, ed. E. N. Parker, C. F. Kennel, and L. J. Lanzerotti, (Amsterdam: North-Holland), 249

Bavassano, B., Dobrowolny, M., Mariani, F., & Ness, N. F. 1982, J. Geophys. Res. 87, 3617

Bavassano, B., Pietropaolo, E., & Bruno, R. 2002, J. Geophys. Res. (Space Physics), 107, 7

Belcher, J. W. & Davis, L. J., 1971, J. Geophys. Res. 76, 3534

Bershadskii, A. & Sreenivasan, K. R. 2004, Physical Review Letters, 93, 064501

Biferale, L. and Toschi,F., 2001, Phys. Rev. Lett., 86 4831

Biferale, L. & Vergassola, M., 2001, Phys. Fluids 13 (8) 2139

Biferale, L., Daumont,I., Lanotte,A. & Toschi,F. 2002, Phys. Rev. E 66, 056306

Biferale, L. & Procaccia, I., 2004, Phys. Rep., submitted, (arXiv:nlin.CD/0404014)

Bruno, R., Bavassano, B., Pietropaolo, E., Carbone, V., & Veltri, P. 1999, Geophys. Res. Lett. 26, 3185

Bruno, R., Carbone, V., Sorriso-Valvo, L., & Bavassano, B., 2003, J. Geophys. Res. (Space Physics), 108, 8

Burlaga, L. F. 1991, J. Geophys. Res., 96, 5847

Burlaga, L. F. 1992, J. Geophys. Res., 97, 4283

Carbone, V. 1993, Physical Review Letters, 71, 1546

Carbone, V., Malara, F., & Veltri, P. 1995, J. Geophys. Res., 100, 1763

Carbone, V., Veltri, P., & Bruno, R. 1995b, Physical Review Letters, 75, 3110

Coleman, P. J. 1966, J. Geophys. Res., 71, 5509

Coleman, P. J. 1968, Astrophys.J., 153, 371

Dobrowolny, M., Mangeney, A., & Veltri, P. 1980, Physical Review Letters, 45, 144

Falkovich,G., Gawędzki, K. & Vergassola, M., 2001, Rev. Mod. Phys. 73, 913

Feynman, J. & Ruzmaikin, A. 1994,

Frisch, U. 1995, *Turbulence. The legacy of A.N. Kolmogorov*, (Cambridge: Cambridge University Press)

Giacalone, J. & Jokipii, J. R. 1996, *J. Geophys. Res.*, 101, 11095

Goldreich, P. & Sridhar, S. 1997, *Astrophysical Journal*, 485, 680

Grappin, R., Leorat, J., & Pouquet, A. 1983, *Astronomy and Astrophysics*, 126, 51

Horbury, T. S. & Balogh, A. 1997, *Nonlinear Processes in Geophysics*, 4, 185

Horbury, T. S. & Balogh, A. 2001, *J. Geophys. Res.*, 15929

Horbury, T. S. & Tsurutani, B. 2001, in *The heliosphere near solar minimum. The Ulysses perspective*, ed. A. Balogh, R. G. Marsden and E. J. Smith. ( London: Springer), 167

Hnat, B., Chapman, S. C., & Rowlands, G. 2003, *Phys. Rev. E*, 67, 056404 *J. Geophys. Res.*, 99, 17645

Iroshnikov, P. S. 1963, *AZh*, 40, 742

Jacob, B., Biferale, L., Iuso, G. & Casciola, C.M., 2004, *Phys. Fluids*, in press

Klein, L. W., Roberts, D. A., & Goldstein, M. L. 1991, *J. Geophys. Res.*, 96, 3779

Klein L.W., Bruno R., Bavassano B., 1993, *JGR* 98 A10, 17,461-17,466

Klein L.W., Roberts D.A., Goldstein M.L., 1991, *JGR* 96 No A3, 3779-3788

Kolmogorov, A.N. 1941, reprinted in *Proc. R. Soc. Lond. A* 434, p. 15 (1991)

Kraichnan, R. H. 1965, *Phys. Fluids*, 8, 1385

Kurien S., & Sreenivasan, K. R., 2000, *Phys. Rev. E* 62, 2206

Lanotte, A. & Mazzino, A., 1999, *Phys. Rev. E* 60, R3483

Leamon, R. J., Smith, C. W., Ness, N. F., Matthaeus, W. H., & Wong, H. K. 1998, *J. Geophys. Res.*, 103, 4775

Marsch, E. & Liu, S. 1993, *Annales Geophysicae*, 11, 227

Matthaeus, W. H., Goldstein, M. L., & Roberts, D. A. 1990, *J. Geophys. Res.*, 95, 20673

Matthaeus, W. H., Oughton, S., Ghosh, S., & Hossain, M. 1998, *Physical Review Letters*, 81, 2056

Ng, C. S. & Bhattacharjee, A. 1996, *Astrophysical Journal*, 465, 845

Parker, E.,N., 1958 *Astrophys.J.*, 128,664-676

Politano, H., Pouquet, A., & Carbone, V. 1998, *Europhysics Letters*, 43, 516

Roberts, D. A., Ghosh, S., Goldstein, M. L., & Matthaeus, W. H. 1991, *Physical Review Letters*, 67, 3741

Ruzmaikin, A. A., Feynman, J., Goldstein, B. E., Smith, E. J., & Balogh, A. 1995, *J. Geophys. Res.* 100, 3395

Shebalin, J.V., Matthaeus, W.H., and Montgomery, D., 1983, *J. Plasma Phys.* 29, 525

Shen, X. & Warhaft, Z., 2000, *Phys. Fluids* 12 (11), 2976

Shen, X. & Warhaft, Z., 2002b, *Phys. Fluids*, 14 (7), 2432

Shen, X. & Warhaft, Z., 2002, *Phys. Fluids* 14 (1), 370

Tu, C. 1988, *J. Geophys. Res.*, 93, 7

Staicu, A., Vorselaars, B., & van de Water,W., 2003, *Phys. Rev. E* 68

Tu, C.-Y. & Marsch, E. 1995, *Space Science Reviews*, 73, 1

Zank, G. P. & Matthaeus, W. H. 1992, *J. Geophys. Res.*, 97, 17189

Table 3. Universality. Scaling exponents, Eqs. (9,11,12)

	$\zeta_2^{aniso}$	$\zeta_4^{aniso}$	$\zeta_6^{aniso}$	$\chi_4^{aniso}$	$\chi_6^{aniso}$
Low-lat	$0.75 \pm 0.15 (xy)$	$0.8 \pm 0.3 (xxxy^\dagger)$	$1.2 \pm 0.4 (xxxyyy)$	$-0.6 \pm 0.2 (xy)$	$-1.2 \pm 0.3 (xy)$
	$0.95 \pm 0.10 (xz)$	$1.0 \pm 0.15 (xzzz)$	$1.2 \pm 0.2 (xxxzzz)$	$-0.8 \pm 0.2 (xz)$	$-1.5 \pm 0.3 (xz)$
	$0.75 \pm 0.10 (yz)$	$1.0 \pm 0.25 (yzzz)$	$2 \pm 1 (yyyzzz)$	$-0.45 \pm 0.2 (yz)$	—
Hi-lat	$0.75 \pm 0.15 (xy)$	$0.8 \pm 0.2 (xxxy^\dagger)$	$1.1 \pm 0.3 (xxxyyy)$	$-0.6 \pm 0.2 (yx^\dagger)$	$-1.1 \pm 0.3 (xy)$
	—	$0.8 \pm 0.3 (xzzz)$	$1.1 \pm 0.3 (xxxzzz^*)$	—	—
	$0.75 \pm 0.15 (yz)$	$1.0 \pm 0.3 (yzzz)$	$1.5 \pm 0.4 (yyyzzz^*)$	—	—

\*Exponents evaluated on the short polar dataset, see Sect. 4.4.

<sup>†</sup>First component provides a third order correlation rather than the second one, as in all other cases considered.